Accountability of the Divertor Power in JET

H J Jäckel, A Chankin, H Falter, G Janeschitz, J Lingertat[1].

JET Joint Undertaking, Abingdon, Oxon, OX14 3EA.
[1] Max Planck Institut für Plasmaphysik, Garching, Germany.

"This document is intended for publication in the open literature. It is made available on the understanding that it may not be further circulated and extracts may not be published prior to publication of the original, without the consent of the Publications Officer, JET Joint Undertaking, Abingdon, Oxon, OX14 3EA, UK".

"Enquiries about Copyright and reproduction should be addressed to the Publications Officer, JET Joint Undertaking, Abingdon, Oxon, OX14 3EA".

Accountability of the Divertor Power in JET

H.J. Jäckel, A.Chankin, H. Falter, G. Janeschitz, J. Lingertat[1]

JET Joint Undertaking, Abingdon, Oxon OX14 3EA, U.K.

[1]*Max Planck Institut für Plasmaphysik, Garching, Germany*

Introduction: In an ideal divertor discharge with the magnetic stagnation point(s) inside the vacuum vessel and no intersection of the scrape-off-layer (SOL) by material components, the target load, P_{cond}^{targ}, is given by

$$\begin{aligned} P_{cond}^{targ} &= P_{cond}^{div} - \alpha\, P_{rad}^{div} - \beta\, P_{CX}^{div} \qquad (\alpha \le 1\ ;\ \beta \le 1) \\ P_{cond}^{div} &= P_{heat}^{bulk} - P_{rad}^{bulk} - P_{CX}^{bulk} - \dot{W}_p \end{aligned} \tag{1}$$

where P_{cond}^{div} is the power conducted into the divertor, P_{heat}^{bulk} the total heating power of the bulk plasma, P_{rad}^{bulk} and P_{CX}^{bulk} the bulk plasma radiation and charge exchange loss (CX), respectively, P_{rad}^{div} the radiation power dissipated in the divertor region and P_{CX}^{div} the CX-power loss in the divertor. The factors α and β account for the the fact, that a certain proportion of the respective losses may be dumped onto the target, according to the divertor geometry and the energy reflection coefficients for particles and photons. We have attempted to reconstruct the target temperature in JET from the conductive target power.

Experimental: The toroidal profile of the JET target has flat and sloped ("ski slopes") regions. The ski slopes cover about 20 % of the total length. The load on the upper (graphite) target can be deduced from three temperature monitoring diagnostics. Absolute temperatures are obtained from a CCD-camera/2,3/ and an IR-camera/4/. The background radiation of a visible spectrometer allows to assess the time history of the temperature qualitatively. The CCD-camera views mainly an inner and outer ski-slope, whereas the IR-camera collect data over flat and sloped parts of the target. The visible spectrometer looks at an outer ski-slope. IR-measurements are not available for the lower (beryllium) target. All three diagnostics have limited dynamic range (CCD: $\Delta T \simeq 600$ C, IR: $\Delta T \simeq 1300$ C). With the CCD and IR-camera only a limited number of discharges were monitored.

Data evaluation: Two different methods have been applied, to evaluate the target load: The target temperature rise, ΔT_{targ}, is calculated from P_{cond}^{targ}, using a simplified one-dimensional model, which disregards lateral heat diffusion.

$$\Delta T_{targ}(t_o) = \frac{1}{f_{targ}} \int_{t_{xp}}^{t_o} \frac{1}{\sqrt{\pi\, k\, \rho\, c}} \frac{P_{cond}^{targ}(t)}{\sqrt{t_o - t}}\, dt \tag{2}$$

The temperature dependent quantities k, ρ and c are the thermal conductivity, the density and the heat capacity, respectively, of the target material, f_{targ} is the effective power deposition area. The bounds of the integral are the time of the onset of the

X-point configuration, t_{xp}, and the current time, t_o. ΔT_{targ} is matched to the temperature rise, absolutely measured by the CCD-camera and qualitatively by the visible spectrometer, by adjusting the wetted area, f_{targ}. When IR-measurements were available, the target load has been deduced from the measured temperature, using the one-dimensional approximation of equation (2). For the calculation of P_{cond}^{targ} in the presented examples, CX-losses have been neglected and $\alpha = 1$ has been assumed. In equation 2, only the triple product $k\,\rho\,c$ is required, not the individual thermal quantities. This product has been deduced from NBI test-bed measurements up to about 1200 C and extrapolated above that temperature.

Results:

Simulation of the target temperature: The measured target temperature can be reconstructed throughout the X-point phase of the discharge from the conductive power, derived with equation 1. However, when high power spikes occur, e.g. at the transition from H- to L-mode or in an X-event, the measured power spikes have to be exaggerated (and can reach $\simeq$100 MW), to match the measured temperature. Figure 1 shows for a high performance single-null (SN) discharge with the X-point at the upper (graphite) target the derived target power, P_{cond}^{targ}, and its simulation, P_{sim}^{targ}, with enhanced power spikes (a). The temperature, T_{sim}^{targ}, is in good agreement with the one, deduced from the background radiation of a visible spectrometer (b) and from the CCD-camera (c). Before about 13.4 s the signal of both diagnostics is within the noise level. The CCD-camera is saturated at 1800 C. The heating power and the stored energy is shown in the bottom box (d).

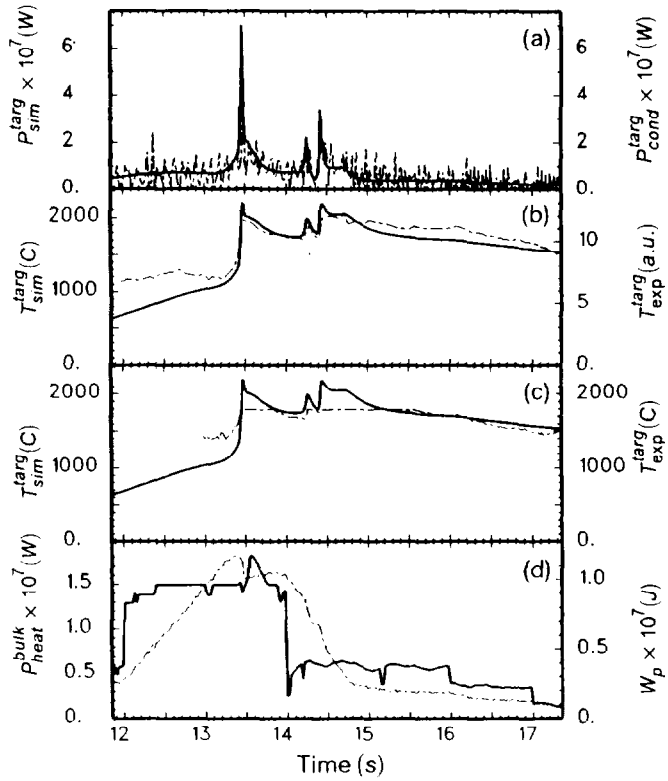

Fig. 1: *Measured, P_{exp}^{targ}, and simulated target power P_{sim}^{targ} (a), from which the evolution of the target temperature, T_{sim}^{targ}, is calculated and compared to experimental data (b,c). Stored energy, W_p, and heating power, P_{heat}^{bulk}, shows the bottom box (d). Solid curves refer to left scales.*

There are several possible reasons for the artificial enhancement of P_{sim}^{targ}. The most obvious is the relatively poor time resolution of the diamagnetic signal of about 30 ms, which at high $\dot{W}_p$ can cause a significant under-estimate of P_{cond}^{targ}. A local thermo-ionic break-down of the sheath at high temperature and accordingly an increase of the conductive power density might be another reason.

Power profiles: Figure 2a shows target temperature profiles, measured by the CCD-camera, of a SN-discharge with the X-point at the lower (beryllium) target at the H- to L-mode transition. The lower detection limit of the camera lies at a temperature of about 850 C. Skewed Gaussians have been fitted to the temperature distribution and from the difference between two subsequent time slices ($\Delta t \simeq 20$ ms) the power deposition profiles have been deduced. The power peaks a few centimeter off the strike points of the seperatrix (dotted vertical lines). The outboard target power is about 40 % higher than the inboard one. The X-point to target distance for this discharge is 8 cm, the direction of the ΔB-drift is towards the target. The half width is $\Delta R^{targ}_{HWFM} \simeq 8$ cm, which would imply a toroidal power deposition area of about 2.5 m^2. For the simulation of the target temperature (fig.1), a wetted area of $f_{targ} = 0.5\ m^2$ has been assumed, which is 20 % of the above estimated area.

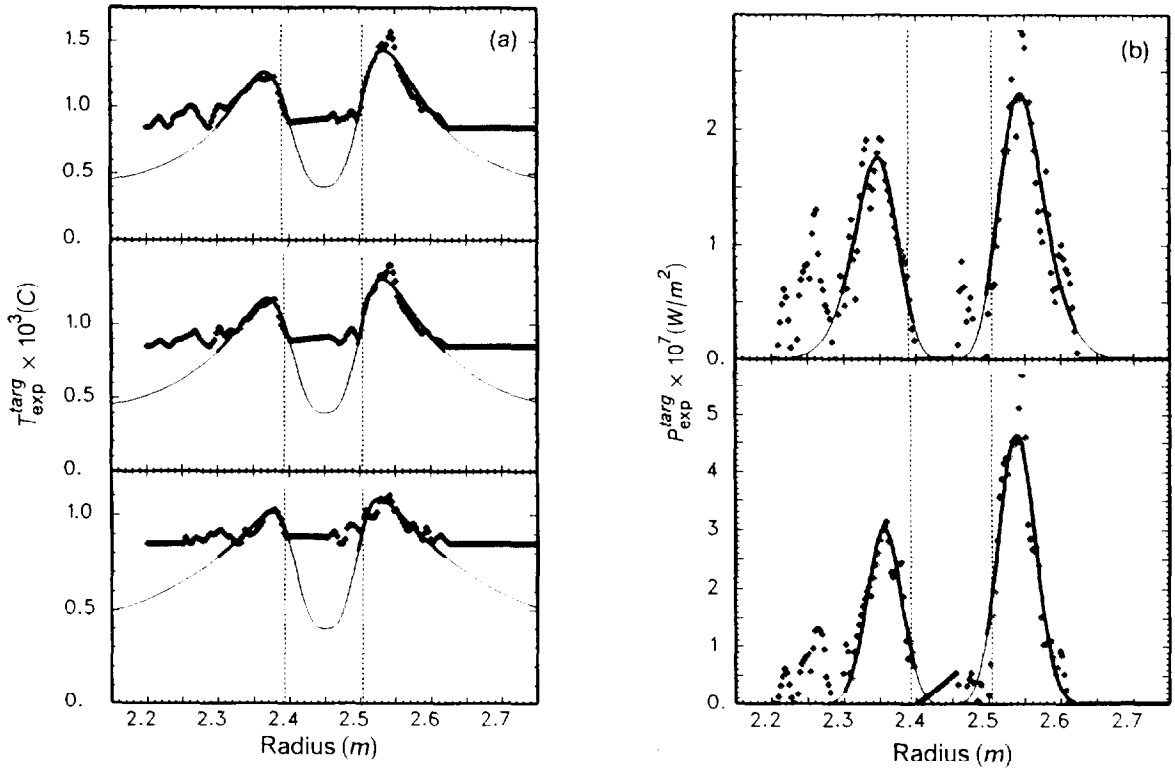

Fig. 2: *Temperature profiles, measured with the CCD-camera, to which skewed Gaussians are fitted (a). The lower detection limit of the CCD-camera is at $T \simeq 850$ C. The deduced power profiles (b) have a radial half width of $\Delta R^{targ}_{HWFM} \simeq 8$ cm and peak close to the strike points of the separatrix (dotted vertical lines).*

Total target power: The total target power, P^{targ}_{exp}, has been deduced from the IR-measurements. A geometrical calibration factor, which relates the viewing area to the total toroidal area has been worked out, which gives reasonable good agreement between the calculated (eq.1), and the experimental target power. Over the range up to $P^{targ}_{cond} \simeq 12$ MW, corresponding to a total heating power $P^{bulk}_{heat} \simeq 22$ MW, a good proportionality between P^{targ}_{cond} and P^{targ}_{exp} is found. Figure 3 shows for 20 discharges with 3 and 4 MA plasma current the measured target load versus the calculated one. About 10 data points are taken at different levels of P^{targ}_{cond} and different confinement regimes of every discharge. At high target power, the

proportionality starts to deteriorate. This is probably due to a beginning of power sharing of the opposite (lower) target. The result is in contrast to findings on DIII-D/5/ ASDEX/6/ and earlier JET/7/ results, where strong non-linearities were found, particular at high heating power. There is at present a yet unresolved discrepancy between the CCD- and the IR-measurements. They both give about the same half widths of the power profiles, but the power maxima, deduced from the IR-measurements are well separated from the strike points, in contrast to the findings from the CCD diagnostic. Unfortunately the same shots have not been monitored with the two diagnostics.

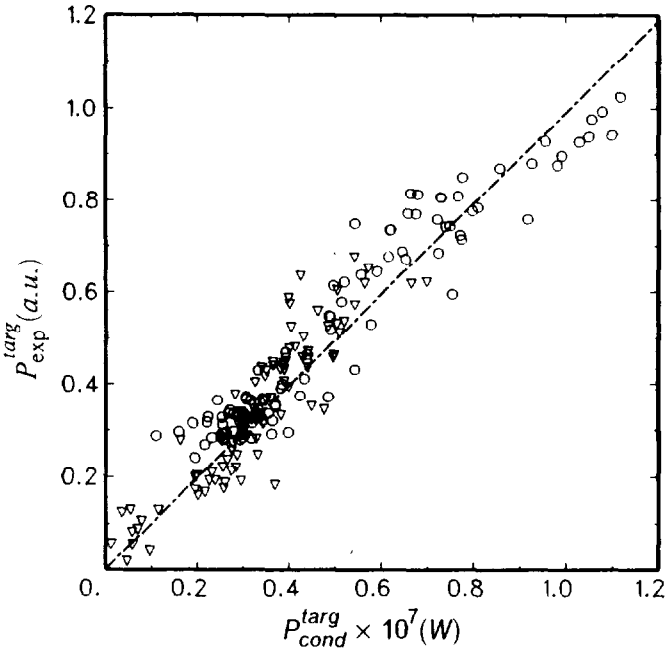

Fig. 3: *Good proportionality is obtained between the calculated (P_{cond}^{targ}) and the measured (P_{exp}^{targ}) target load. The data cover the H-mode as well as the L-mode phase of discharges with 3 MA (triangles) and 4 MA (circles) plasma current.*

Conclusions:

- The measured target temperature can qualitatively be simulated with the power conducted to the target. However, at fast changes in the confinement, the resulting power spikes have to be enhanced to match the measured temperature rise. These power spikes can reach about 100 MW.
- A half width of the target power profiles of $\Delta R_{HWFM}^{targ} \simeq 8$ cm is derived from experimental data.
- IR-measurements infer a linear relation between measured and calculated target power, in contrast to probe measurements in the target.
- There seems to be no significant difference in the power accountability between the L-mode and the H-mode phase.

References:

/1/ *A.Loarte, P.J.Harbour, Nucl. Fusion 32(1992) 681.*
/2/ *J.Lingertat et al., this conference*
/3/ *R.Reichle, D.D.R.Summers and M.F.Stamp, J. Nucl.Mater. 176&177(1990) 375*
/4/ *A.Chankin et al., to be published.*
/5/ *A.W.Leonhard et al., 34th Annual Meeting of the APS (1992), Seattle, USA*
/6/ *ASDEX Team, Nucl. Fusion 29(1989) 1959.*
/7/ *A.Loarte, PhD-Thesis, Universidad Complutense de Madrid, 1992*